Article

Modulation Effect of Mesoscale Eddies on Sequential Typhoon-Induced Oceanic Responses in the South China Sea

Weifang Jin [1], **Chujin Liang [1]**, **Junyang Hu [1]**, **Qicheng Meng [1]**, **Haibin Lü [2]**, **Yuntao Wang [1],***, **Feilong Lin [1]**, **Xiaoyan Chen [1]** and **Xiaohui Liu [1]**

[1] State Key Laboratory of Satellite Ocean Environment Dynamics, Second Institute of Oceanography, Ministry of Natural Resources, Hangzhou 310012, China; jinweif@sio.org.cn (W.J.); cjliang@sio.org.cn (C.L.); junyanghu@sio.org.cn (J.H.); q.meng@sio.org.cn (Q.M.); lfl@sio.org.cn (F.L.); chenxy@sio.org.cn (X.C.); xh_liu@sio.org.cn (X.L.)

[2] Jiangsu Key Laboratory of Marine Bioresources and Environment/Jiangsu Key Laboratory of Marine Biotechnology, Jiangsu Ocean University, Lianyungang 222005, China; haibin_lv@jou.edu.cn

* Correspondence: yuntao.wang@sio.org.cn; Tel.: +86-571-8196-3629

check for updates

Abstract: The impacts of mesoscale eddies on the modulation of typhoon-induced oceanic responses are important for understanding ocean dynamics. Satellite observations identified prominent ocean surface temperature and chlorophyll changes over the regions with mesoscale eddies after two sequential typhoons, e.g., Linfa and Nangka, in the South China Sea. The impacts of typhoons on the ocean surface were more prominent within cyclonic eddies than within anticyclonic eddies. The wind speed (translation speed) of Linfa was much larger (slower) than that of Nangka; thus, the changes induced by Linfa were stronger. However, the second typhoon easily generated mixing through the weak stratification induced by the first typhoon and impacted the upper ocean. The strong chlorophyll enhancement induced by Nangka was identified at a cyclonic eddy. Using a combination of reanalysis data, the depth of water origin (DWO) was applied to quantify the depth to which a typhoon's impact could be exerted. Prominent changes were identified when the DWO reached the depth at which the temperature and nutrients differed from those within the mixed layer. This method can overcome the impacts of cloud coverage when examining a typhoon's influence with remotely sensed data and offers a quantitative approach to determine the mechanisms responsible for typhoon-induced ocean surface changes.

Keywords: mesoscale eddies; sea surface chlorophyll; typhoon; South China Sea; sea surface temperature; depth of water origin

1. Introduction

Tropical cyclones, which present as intense and devastating atmospheric events, are generated mainly near the tropics and propagate to midlatitudes [1]. The tropical cyclones generated in the northwestern Pacific Ocean, known as typhoons, account for more than 1/3 of all tropical cyclones in the Northern Hemisphere annually [2]. During their movement, typhoons can induce significant impacts on the upper ocean by driving the motions of waters beneath [3], e.g., large typhoon winds generate strong vertical mixing and upwelling within the ocean, which brings subsurface cold, high-nutrient water to the surface [4]. A cold surface is formed in front or at the wake of the typhoon path [5]. Consequently, the cold surface temperature modifies the typhoon intensity by blocking the following typhoons from gaining energy from the warm ocean surface [6,7]. Thus, single typhoons usually

trigger substantial sea surface cooling and sea surface chlorophyll (CHL) blooms [8,9], but the impacts of sequential typhoons are much less pronounced [10].

Typhoon-induced ocean responses vary greatly depending on the typhoon's features (e.g., wind speed, pressure, and translation speed) and the preconditions of the upper ocean (e.g., mesoscale eddies, thermocline, mixed layer depth and strength of stratification) [1,11]. Strong winds during typhoons induce intensive mixing, which largely influences the upper ocean [12]. The wind stress curl associated with atmospheric cyclonic motions can drive substantial Ekman pumping, leading to upwelling beneath the typhoon center [13]. Both mixing and upwelling can occur simultaneously, and their relative importance is different in each case [2]. In general, strong-intensity and slow-moving typhoons are expected to induce large responses [14]. Numerous studies have investigated the impacts of typhoons on the ocean, including the spatial extent and temporal dependence of the typhoon's influence. For instance, typhoons can stimulate strong winds and wind–current resonance on the right side of the typhoon's track, resulting in stronger mixing than on the left side [4,9]. Moreover, the temperature changes instantly as the typhoon approaches, whereas CHL blooms are usually delayed [15]. This difference is attributed primarily to wind-induced mixing, which decreases temperature and elevates nutrients within a few hours [13], while the growth of phytoplankton takes several days [3]. On the other hand, CHL enhancement can be associated with cooling temperatures when typhoons bring subsurface CHL maxima directly to the surface [16].

The status of the ocean can also influence the oceanic responses to typhoons; previous studies generally described the changes near the surface, although the vertical structure of the water column and the depth of typhoon-induced mixing are particularly important [17]. Large ocean responses are found in regions with strong vertical gradients, and stratification is greatly reduced during the passage of a typhoon [18]. Because the temperature usually decreases monotonically with depth, stronger responses occur when mixing reaches greater depths [2]. The variability in CHL is more complex than that in temperature. In general, the nutrient content is low within the mixed layer depth (MLD) that the growth of phytoplankton is limited by the availability of nutrients, leading to low CHL levels [19]. As the nutrient content gradually increases with depth, CHL also slightly increases [20]. The nutrient level is much larger beneath the nutricline; however, the growth of phytoplankton is limited by the availability of light [21]. A subsurface CHL maximum (SCM) is usually identified within the euphotic zone around the nutricline, where both the nutrient level and the availability of light can barely support phytoplankton growth [8]. Thus, CHL is simultaneously modulated by nutrients and light, and the nutrients within the euphotic zone can be greatly elevated when typhoon-induced vertical mixing deepens the MLD [22]. Although the typhoon-induced mixing depth and upwelling velocity can be estimated [23], it is fundamentally important to gauge whether subsurface cold and high-nutrient water can be lifted to explicitly assess the responses of upper ocean.

As a ubiquitous dynamic feature, mesoscale eddies are characterized by intensive vertical dynamics and can modulate ocean responses to typhoons. Cyclonic (anticyclonic) eddies are characterized by upwelling (downwelling) within their interior [24]. A previous study revealed that the responses of the ocean to typhoons can be intensified (suppressed) by cyclonic (anticyclonic) eddies because the elevated (depressed) MLD via central upwelling (downwelling) can be enhanced (reduced) by typhoons [13]. Thus, pre-existing eddies can alter the intensity of temperature cooling and enhancement in CHL [25–27]. A previous study identified that a weak typhoon can still induce large and long-lasting oceanic responses in a pre-existing cyclonic eddy [13]. Other studies suggested that only 18% of typhoons can induce CHL enhancement, even with ubiquitous eddies [28]. Therefore, in addition to the importance of typhoon features and oceanic status, mesoscale eddies contribute to the large discrepancies among typhoons in different oceans, which requires further explanation.

Every year, a substantial number of typhoons pass through the South China Sea (SCS), a semienclosed ocean basin in the northwestern Pacific Ocean [16]. Because the nutrient level is extremely low at the ocean surface, the SCS is classified as a typical oligotrophic zone, although solar radiation is strong throughout the year with a euphotic zone that can extend up to 100 m [29].

A prominent seasonal cycle of typhoon occurrence is identified that strong and frequent typhoon activities occur from spring to fall [30]. During this period, the MLD is very shallow, ranging between 20 m and 40 m [31]. Moreover, the nutricline and SCM are highly consistent with each other, located near a depth of 60 m [32]. Numerous studies have been conducted in the SCS to investigate the impacts of typhoons on the ocean surface, and these studies revealed that typhoons can significantly change the ocean status [3]. Predominant mesoscale eddies are observed within the SCS, occupying approximately 25% of the ocean surface on average [33]. Previous studies have revealed that mesoscale eddies in the SCS can greatly modulate typhoon-induced ocean surface responses [11,22,34,35]. The SCS is a good study site with abundant typhoon events and complex oceanic dynamics, e.g., ubiquitous eddies, that can help to quantitatively disentangle typhoon-induced oceanic responses. Specifically, Chen and Tang [36] found that cyclonic eddies enhanced ocean responses during the passage of typhoon Linfa in 2009. This phenomenon mainly occurred because eddy-induced upwelling is enhanced by strong winds [37]. As eddies rapidly advect upwelled high-nutrient water to the surroundings, the induced phytoplankton bloom at the surface can last for a long period. However, a typhoon occurred immediately after Linfa, which was not identified in the former study [36]. The dynamics of sequential typhoons can be quite different from those of a single typhoon, and thus, this scenario should be further investigated.

Multiple observational methods, e.g., Argo floats, satellites and moorings, have been applied to study the responses of typhoon-impacted oceans. Argo profiles describe the changes in the vertical structure of the water column during typhoons, and satellites capture the features of the ocean surface [2,36]. Numerical modeling and reanalysis datasets are highly valuable for further resolving the three-dimensional processes and offer quantitative descriptions of typhoons' impacts [38]. Our understanding of ocean dynamics under the impact of a typhoon has been greatly improved. However, the situation can become very complex when different conditions are encountered simultaneously. For example, sequential typhoons passing over the ocean with mesoscale eddies are a perfect example to study ocean dynamics, but such events have rarely been identified. Hence, the tandem effects of typhoons and eddies on the sea surface in the SCS are an interesting topic that needs further exploration. In this study, the impacts of typhoons on the ocean surface in the SCS modulated by mesoscale eddies with different polarities are investigated. A universally applicable method based on a three-dimensional reanalysis dataset is proposed to quantitatively gauge typhoon-induced upper ocean responses. The remainder of this paper includes five sections: Section 2 describes the information on the typhoons and the materials and methods used in this study; the typhoon's impacts on the ocean in the SCS and the underlying eddy-induced dynamics are shown in Section 3; a comprehensive analysis of the typhoon-induced dynamics is presented in Section 4, followed by a summary in Section 5.

2. Data and Methods

The typhoon information was obtained from the Japan Meteorological Agency (JMA, http://www.jma.go.jp/jma/indexe.html). These data include the maximum sustained wind (MSW), category and location (longitude and latitude) of the typhoon center every 6 h. The category of typhoons is defined following the rule of the JMA that the MSWs of a tropical cyclone at category-3 and category-4 are between 17 m/s and 24 m/s and between 25 m/s and 32 m/s, respectively. The applied category in current study is different from the international categorization, which corresponds to tropical storm and severe tropical storm, respectively. The translation speed (Uh, m/s) of the typhoon was calculated as the ratio between the spatial distance traveled between two successive typhoon centers and the corresponding time span. The daily wind fields were obtained as the average of two satellite observational datasets. The first dataset was measured by the SeaWinds microwave scatterometer onboard the Quick Scatterometer (QuikSCAT, https://winds.jpl.nasa.gov/) satellite with a spatial distribution of 0.25° × 0.25°. To compensate for some observational gaps in the wind field, the other dataset from the Advanced Scatterometer (ASCAT), which was developed by the European Organisation

for the Exploitation of Meteorological Satellites (EUMETSAT, http://www.remss.com/missions/ascat/), was applied.

Daily sea surface temperature (SST) data with a resolution of 0.25° × 0.25° was measured by the Advanced Very High-Resolution Radiometer (AVHRR) onboard the Polar-Orbiting Environmental Satellites, which was obtained from the National Centers for Environmental Information (NCEI, https://www.ncei.noaa.gov/). The corresponding climatology was calculated as the 15-year average ranging between 2002 and 2016 for each date over the year. Daily remotely sensed CHL concentrations with a spatial resolution of 4 km developed by the European Space Agency (ESA) Ocean Color Climate Change Initiative (OC-CCI, http://www.oceancolor.org/) are used to investigate the spatial and temporal variations in the phytoplankton biomass at the sea surface. Correspondingly, the daily CHL climatology is calculated on each day of the year using the same 15-year dataset.

Archiving, Validation and Interpretation of Satellite Oceanographic (AVISO) sea level anomaly (SLA) data with a spatial resolution of 0.25° × 0.25° was downloaded from the Copernicus Marine Service (CMEMS, http://marine.copernicus.eu/). The SLA data is used to derive the geostrophic current and to detect mesoscale eddies following Chelton et al. [24]. Specifically, pre-existing oceanic eddies are identified based on the sea surface height anomaly (SSHA) as follows: a local peak (trough) of SLA is first found, and the largest closed contours of SLA with a single regional maximum (minimum) are defined as anticyclonic (cyclonic) eddies. The anticyclonic eddies are characterized by a positive SLA (>5 cm) relative to the surroundings, while cyclonic eddies have a negative relative SLA (<−5 cm) [39].

A reanalysis dataset of the three-dimensional daily ocean temperature, salinity and derived density was extracted from the Global Ocean Forecasting System (GOFS) 3.1 reanalysis product based on the Hybrid Coordinate Ocean Model (HYCOM, http://apdrc.soest.hawaii.edu/). This dataset has a spatial resolution of 1/12° × 1/12° and 30 layers in the vertical direction. A detailed description can be found in Vidya et al. [40]. The product was forced by the Navy Operational Global Atmospheric Prediction System [41] and adjusted by the data assimilation system to produce a 3D variational scheme [42]. The assimilative data sources include satellite altimeter observations, satellite SST, and in situ vertical temperature and salinity profiles from expendable bathythermographs (XBTs), Argo floats and moored buoys. The MLD is calculated as the depth where the water temperature is 0.55 °C cooler than the corresponding temperature at the surface [12].

3. Results

3.1. Typhoons' Impacts on the Ocean Surface

Two sequential but weak typhoons, Linfa and Nangka, passed over the SCS in June 2009 (Figure 1). Typhoon Linfa was generated in the middle of the SCS on 17 June 2009; it remained near its origin for another day before moving northward on 19 June. The translation speed was approximately 2.3 m/s during this period. The typhoon was first classified as category 2 (tropical depression, MSW < 17 m/s) and was gradually increased to category 3 (tropical storm, 17 m/s < MSW < 24 m/s) and category 4 (severe tropical storm, 24 m/s < MSW < 32 m/s) before it entered the East China Sea on 21 June [43]. Typhoon Nangka originated in the western Pacific (10.8°N, 129.0°E) on 22 June with a wind speed of 18 m/s, after which it moved northwestward across the Philippines and entered the SCS on 24 June as a category-3 typhoon. In the following days, the typhoon moved rapidly towards the northwest at a maximal wind speed of 20.6 m/s until making landfall in Guangdong Province on 26 June. The averaged translation speed of Nangka was 6.2 m/s, which was substantially larger than that of Linfa. The wind speed for Linfa was slightly larger than that for Nangka, although both were characterized by relatively small MSW (less than 32 m/s). Both events passed over the SCS, as denoted by the dashed box in Figure 1a, and the occurrences of these typhoons were temporally separated by approximately a week. The water depth is more than 1000 m in the central SCS and gets shallower towards the coast. The corresponding climatological SST and CHL in June decreases and increases, respectively, from south to north (Figure 1b), although the spatial variance is actually small.

In particular, for the region impacted by both typhoons, the SST is approximately 29.4 °C, and the CHL is close to 0.07 mg/m^3.
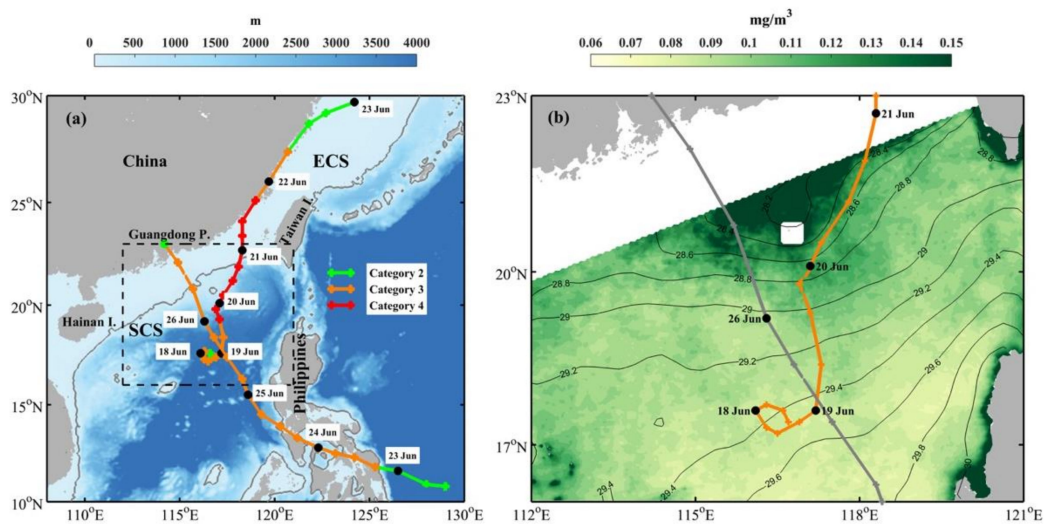

Figure 1. (**a**) Map of the South China Sea (SCS) and East China Sea (ECS) with 200-m isobath; and the trajectories of the two typhoons. The 00:00 time on each day is labeled at the locations of the typhoons. The typhoon category, which is based on JMA (Japan Meteorological Agency) categorization, is represented by the color. The study region is delineated by the dashed black square. (**b**) Climatological average of the sea surface chlorophyll (CHL, shading, mg/m^3) and sea surface temperature (SST, contours, °C) in June. The trajectories for typhoons Linfa and Nangka are shown in orange and gray, respectively. The values over the region close to the coast and island are masked. The SST and CHL data are respectively obtained from Ocean Color Climate Change Initiative (OC-CCI) and Advanced Very High-Resolution Radiometer (AVHRR).

The typhoons dominate the wind patterns throughout the study region during the period as they pass over the SCS (Figure 2). The wind speed intensity is roughly the same from 17 June to 20 June for Linfa; the wind fields on 19 and 20 June are shown to be associated with large Ekman pumping velocities (EPVs) within the typhoon center that are approximately 11.0×10^{-4} m/s and 15.7×10^{-4} m/s, respectively. For Nangka, the wind fields on 25 June and 26 June are shown since the typhoon rapidly traverse the study region, and the corresponding EPVs are 4.8×10^{-4} m/s and 8.1×10^{-4} m/s, respectively. Compared with those for Linfa, the wind intensity and EPV for Nangka are prominently smaller. The average typhoon radii of Linfa and Nangka with wind speeds of 15 m/s are 200 km and 250 km, respectively, when they are within the study region (Figure 3a,c).

Prominent SST cooling and CHL enhancement are identified along the typhoons' tracks within the typhoon-impacted area (Figure 3). The typhoon-induced ocean surface change is obtained as the average of several days' anomalies after the typhoons, where an anomaly is defined as the difference between the ocean surface parameter and the corresponding climatology. Because the times required for the SST and CHL to respond after a typhoon vary from each other [5,44], the selected time period should be different. In this study, the SST (CHL) is calculated over the period from 20 June to 22 June (20 June to 25 June) for Linfa and from 25 June to 27 June (26 June to 1 July) for Nangka. Some studies obtained the typhoon-induced changes as the difference between the time series after and before the typhoon [35]. Because the seasonal variability is prominent for entire period over two typhoons [22], the daily climatology is removed instead to obtain the anomalous field. The impacts of the typhoons on the SST are clearly captured, and prominent cooling can be found along their tracks, particularly on the right side. CHL enhancement can be found along the tracks as well, although the right-side bias is less prominent than with the SST. Because the CHL change is much larger in the coastal region than in the open ocean, the region within 200 km from the coast is masked to highlight the typhoon-induced CHL

changes offshore. Linfa induces larger impacts on the SST and CHL than Nangka; e.g., the largest SST cooling is approximately −4 °C and −2 °C for Linfa and Nangka, respectively, and the corresponding maximum CHL enhancements are 0.5 mg/m^3 and 0.2 mg/m^3.
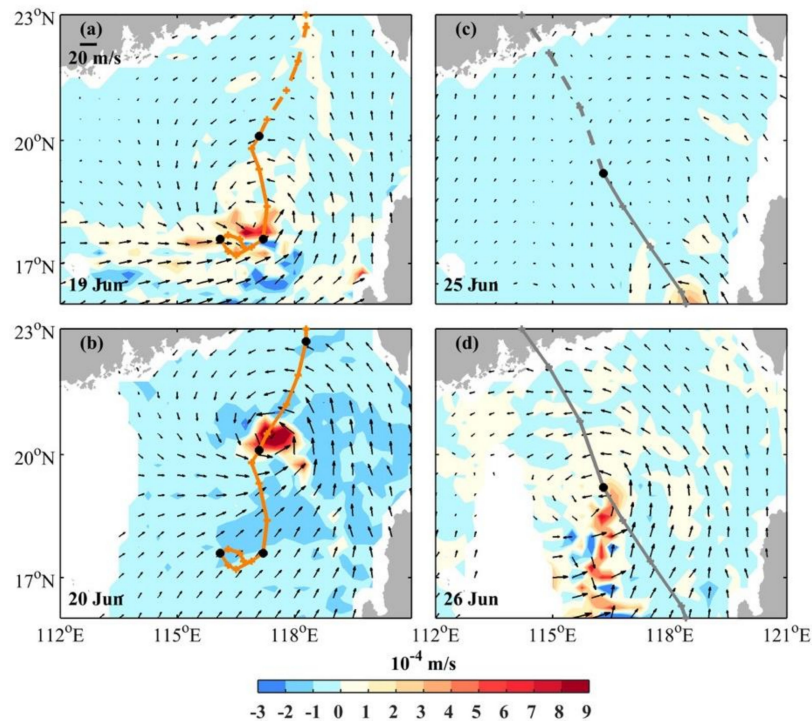

Figure 2. Wind field (vector, m/s) overlaid with the Ekman pumping velocity (shading, m/s) for typhoon Linfa on (**a**) 19 June and (**b**) 20 June and for typhoon Nangka on (**c**) 25 June and (**d**) 26 June. The typhoon trajectory after the depicted date is shown as a dashed line.
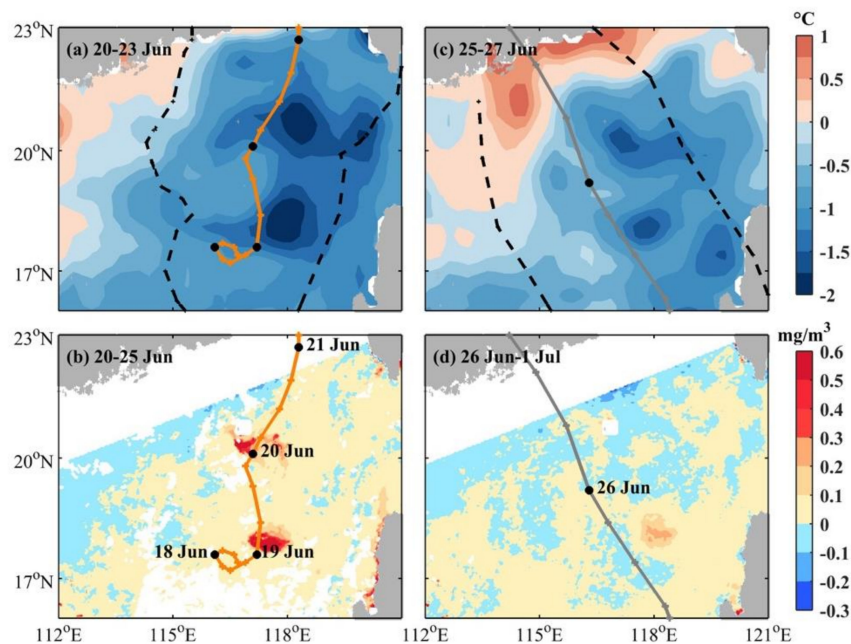

Figure 3. Changes induced by typhoons Linfa (**a**,**b**) and Nangka (**c**,**d**) in the (**a**,**c**) sea surface temperature and (**b**,**d**) sea surface chlorophyll. A change is defined as the average anomaly, which is the difference between the daily observations and corresponding climatology during the period denoted in each panel. The radius of the typhoon speed equal to 15 m/s is shown as dashed black lines.

3.2. Modulation Effect of Eddies on Typhoon-Induced Cooling

There are two zones featuring SST cooling greater than −2 °C centered at 17.7°N, 117.6°E and 20.1°N, 117.4°E, where strong responses are identified along the track of Linfa. The two areas are approximately circular with radii equal to 160 km and 110 km. As depicted in the mean SLA field between 18 June and 27 June, these areas correspond to the occurrence of two cyclonic eddies (Figure 4). Both eddies are similar in size, but the northern eddy (CE1) has a strong intensity and is less impacted by surrounding eddies; detailed information on both eddies during the passage of typhoons can be found in Table 1. Here, the relative SLA is defined as the difference between the maximum SLA within the eddy and the SLA averaged around the eddy perimeter, whose value is positive (negative) for anticyclonic (cyclonic) eddies. During the same period, two anticyclonic eddies are also located near the typhoons' tracks. The southern region (ACE2) is characterized by a strong intensity with a radius equal to 86.4 km and a relative SLA of approximately 10.7 cm. In contrast, the northern anticyclonic eddy (ACE1) is located between cyclonic eddies with a small radius and magnitude (Table 1). The longevity of ACE1 is much shorter than that of other eddies, as it fades on 27 June when immersed by CE2 (not shown). The eddies are generally located to the right of both typhoons' trajectories; the only exception is Nangka, which passes immediately over the southern anticyclonic eddy (ACE2). The four identified eddies pre-existed in the SCS before Linfa and remained after Nangka, and they have very important impacts on the vertical structure of the water column and typhoon-induced variation, which will be described later. Although some other eddies can be identified as well, such as the one centered at 18°N, 115.3°E, they are far from the typhoons and less prominently impact the ocean surface.
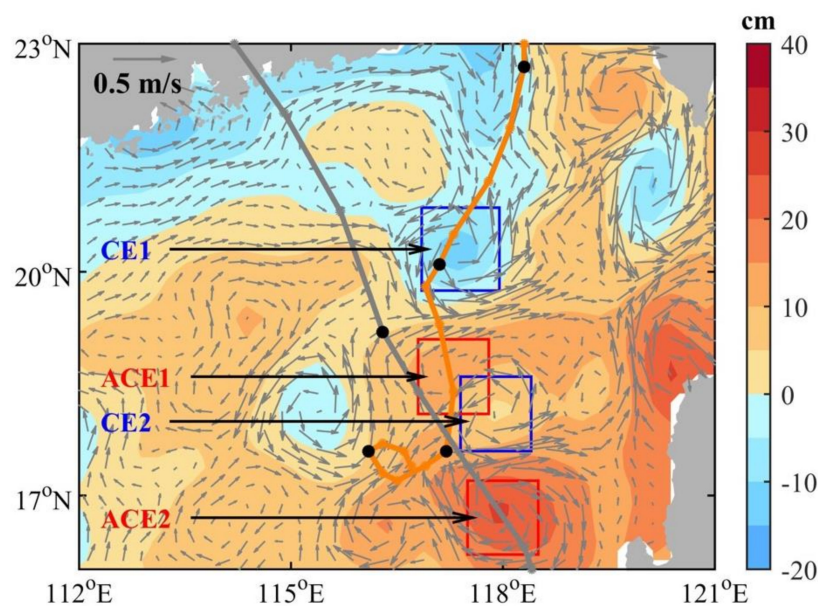

Figure 4. The averaged sea level anomaly (shading, cm) and geostrophic current (vector, m/s) between 18 June and 27 June. The selected locations for cyclonic eddies (blue) and anticyclonic eddies (red) are labeled along the typhoon's trajectories.

Table 1. Information on all eddies during the passage of typhoons (CE: cyclonic eddy; ACE: anticyclonic eddy; SLA: sea level anomaly; TY: typhoon).

		CE1	CE2	ACE1	ACE2
	Period	10 June–31 July	19 June–16 July	10–27 June	18 May–28 July
	Region of eddies	116.8–117.9°E 19.7–20.8°N	117.4–118.4°E 17.6–18.6°N	116.8–117.8°E 18.1–19.1°N	117.5–118.5°E 16.2–17.2°N
	Area of eddies (km²)	13,981	11,718	11,684	11,811
Linfa (17–23 June)	Averaged position	117.5°E 20.5°N	117.8°E 18.2°N	117.5°E 18.6°N	118.0°E 16.8°N
	Averaged radius (km)	63.1	54.8	57.2	86.4
	Maximum relative SLA (cm)	−7.8	−5.7	7.4	10.7
	Smallest distance to TY (km)	4.75	45.34	11.48	108.90
Nangka (24 June–2 July)	Averaged position	117.3°E 20.0°N	117.8°E 18.2°N	17.5°E 18.7°N	118.0°E 16.8°N
	Averaged radius (km)	74.9	78.2	40.0	68.8
	Maximum relative SLA (cm)	−7.4	−5.6	0.6	11.6
	Smallest distance to TY (km)	112.36	65.22	65.50	4.08

The temporal dependence of the typhoon-induced ocean surface responses is further investigated at the location of each eddy (Figure 5). The wind speed starts to increase before Linfa's arrival on 17 June and reaches a maximum, e.g., approximately 18 m/s at CE2, during its passage. The daily wind speed is obtained by averaging the wind within the area of the eddy; thus, the value is less than the MSW. The difference in time when the wind speed reaches its peak is clearly related to the locations of the eddies, which appear in the order of ACE2, CE2, ACE1 and CE1 from south to north (Table 2). While the peak value of the wind speed is related to the distance between the eddies and typhoon center, the wind in ACE2 is clearly weaker, e.g., approximately 15 m/s, because the eddy is farther from the typhoon track (Table 1). For Nangka, the wind speed starts to increase on 25 June upon entering the SCS and rapidly reaches a peak on 26 June before decreasing back to its normal speed. The wind speed during Nangka is prominently weaker than that during Linfa, with the former reaching a maximum of approximately 12 m/s. Comparing the wind speeds among the different eddy locations, their time series are highly similar because Nangka traverses the study region in a very short period. The winds during the time period between the two typhoons are characterized by slow speeds, and the corresponding values are comparable to the normal status.

The SST decreases prominently for all eddies simultaneously with the increases in the wind speed between 16 June and 21 June for all eddies. The cooling in the CE2 is more than −2 °C, which is more prominent than that in the anticyclonic eddies, with a decrease close to −1.5 °C. The SST cooling trend relaxes as the typhoon passes over the SCS on 21 June, but surface cooling can still be identified during the following three days. As Nangka arrives on 25 June, it instantly stimulates another surface cooling event. The SST depression is weak but recognizable compared with the cooling induced by Linfa, and the SST decreases are comparable among all the eddy locations. The SST increases back to its climatological value over the four days after Nangka passes through the study area. CHL enhancement is captured for all eddies after Linfa except ACE2; in contrast, after Nangka, a bloom is identified for only CE2. The CHL change is prominently delayed by a few days compared with the delay in the SST change.

From 23 to 24 June, 3 days after Linfa, a weak CHL bloom (e.g., 0.03 mg/m^3) can be identified for ACE1, while large CHL blooms (e.g., 0.2 mg/m^3) are found in the cyclonic eddies. Interestingly, after Nangka, another CHL peak is observed at CE2 with an enhancement of approximately 0.14 mg/m^3, but no CHL change is associated with the other eddies. This difference occurs because the three-dimensional processes cannot be captured from satellites. The CHL in the cyclonic eddies relaxes back to the climatological average on 2 July, approximately one week after Nangka. On the other hand, the CHL in the anticyclonic eddies is persistently higher than the climatological average during the study period, which may be due to the advection of surrounding water with a high CHL content from CE2. In summary, the modulation effect of eddies on typhoon-induced changes at the ocean surface is prominent, as will be discussed in the following section.
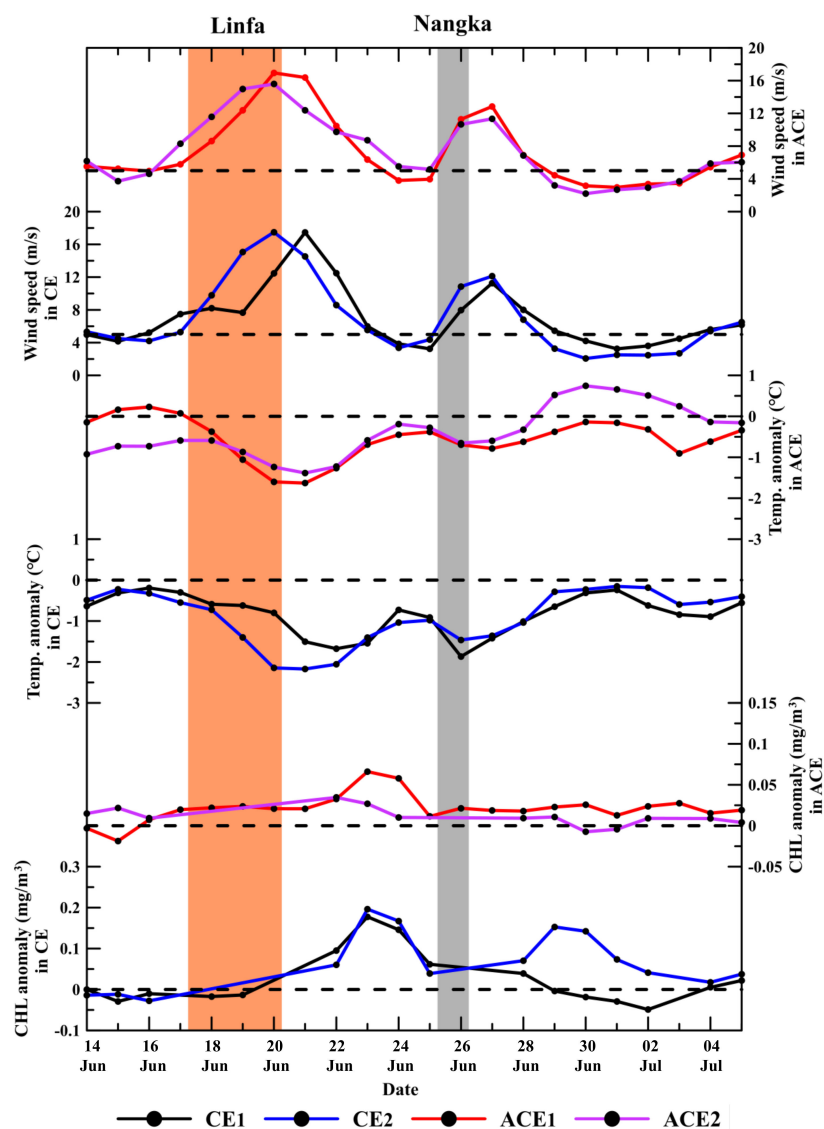

Figure 5. Time series of the wind speed (m/s), temperature anomaly (°C, AVHRR) and CHL anomaly (mg/m^3, OC-CCI) at CE1 (black), CE2 (blue), ACE1 (red) and ACE2 (magenta). The periods for Linfa and Nangka are indicated by the orange and gray bands, respectively. The averaged wind speed is shown as horizontal dashed lines. The anomaly field is obtained as the difference between the daily observations and the corresponding climatology between 8 June and 7 July.

Table 2. Typhoon-induced ocean changes at all eddy locations.

		CE1	CE2	ACE1	ACE2
Linfa	Period when typhoon passed over the eddy	18 on 19 June–00 on 20 June	00–06 on 19 June	06–12 on 19 June	06 on 17 June–00 on 19 June
	Maximum ΔT (°C)	−1.68	−2.17	−1.63	−1.38
	Time for maximum ΔT	22 June	21 June	21 June	21 June
	Maximum ΔCHL	0.17	0.20	0.07	0.03
	Time for maximum ΔCHL	23 June	23 June	23 June	22 June
Nangka	Period when typhoon passed over the eddy	00–06 on 26 June	18 on 25 June–00 on 26 June	12–18 on 25 June	06–12 on 25 June
	Maximum ΔT (°C)	−1.86	−1.46	−0.78	−0.65
	Time for maximum ΔT	26 June	26 June	27 June	26 June
	Maximum ΔCHL	0.04	0.15	0.03	0.01
	Time for maximum ΔCHL	28 June	29 June	30 June	29 June

The vertical sections of the water columns within the eddies are further investigated to understand the dynamics therein. Reanalyzed data from HYCOM are applied with the MLD depicted for each location in Figure 6. The initial MLDs are approximately 20 m at all locations, and the MLD starts to deepen when the typhoon arrives, associated with the occurrence of upwelling. The MLD and upwelling continue to increase until two days after the typhoon, characterized by prominent SST cooling. Subsequently, the temperature within the top 20 m increases, associated with shoaling of the MLD, which can rebound back to an even shallower depth than that under pre-typhoon conditions. The shallowest MLD is generally observed when Nangka arrives on 24 June, which induces further mixing. Although the wind speeds during Nangka are much weaker than those during Linfa, the maximum induced MLD, which also takes place two to three days after Nangka, is similar to or even larger than the maximum MLD after Linfa. Then, the MLD becomes very shallow and remains so for approximately four days, and after 2 July, the MLD deepens to a depth similar to the initial value.
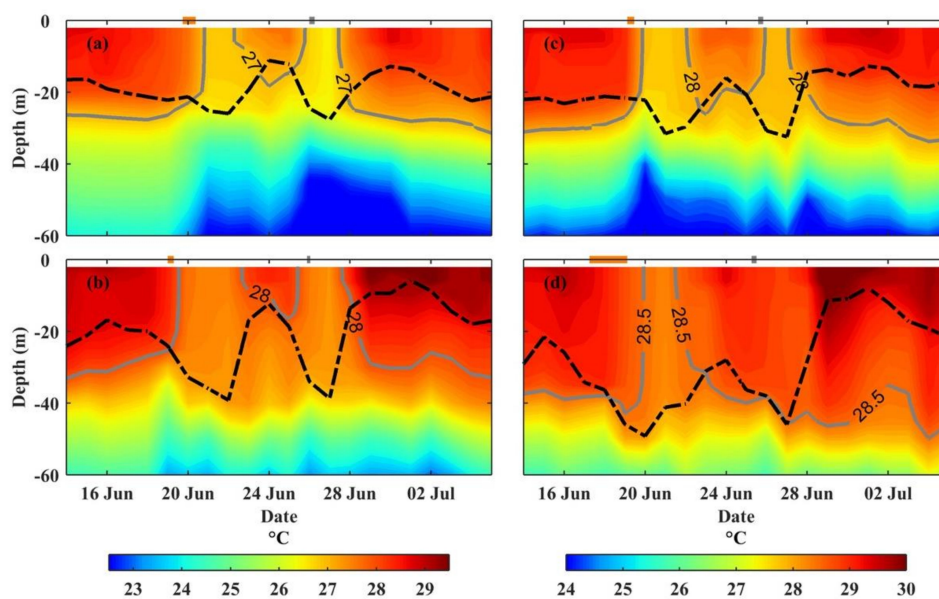

Figure 6. Time series of the temperature profile with isobaths of 27 °C, 28 °C, 28 °C and 28.5 °C for (**a**) CE1, (**b**) CE2, (**c**) ACE1 and (**d**) ACE2, respectively. The dashed black lines indicate the mixed layer depth. The horizontal bars represent the duration of each typhoon.

　　　The climatological profiles of temperature and nutrients are averaged for June over the region covering all identified eddies (Figure 7b,c). The calculated MLD is 20 m, where the temperature is 0.55 °C less than the SST following Obata et al. [45]. The temperature is well mixed above the MLD with a value of approximately 29 °C and monotonically decreases beneath the MLD. On the other hand, the nutrient concentration is extremely low at the surface and persistently lower than 0.5 μM within 50 m of where the nutricline is identified [46], while a prominent nutrient increase is identified beneath the nutricline. Upon comparing the profiles at different eddy locations with each other, the patterns are highly similar within the top 50 m, which can be confirmed by the small standard deviations. The depth of water origin (DWO) is obtained by comparing the SST with the climatological temperature profile, where the upwelling origin is defined as the depth where the climatological water temperature is similar to the SST. If the SST is warmer than the climatological surface temperature, the DWO is defined as zero. Although the depth influenced by EPV and mixing can be estimated using wind stress, the upper ocean structure is largely different and can impact the influenced depth [40]. The advantage for the application of DWO is that the reanalyzed dataset offers a near real-time description of the ocean status [42] that considers the vertical variation. The DWO time series is shown for all eddy locations (Figure 7a), and the general patterns are similar to the variations in the MLD. For cyclonic eddies, the surface water always originates from the subsurface due to eddy-induced persistent upwelling. Before the arrival of Linfa, the DWO is approximately −12 m and −30 m for CE1 and CE2, respectively. As Linfa moves across the study region, the DWO gradually increases to greater depths, and the maximum depths are −30 m and −40 m for CE1 and CE2, respectively, on 22 June. The DWO subsequently shallows as the wind-induced mixing is reduced; however, the DWO deepens again when Nangka arrives on 24 June. The Nangka-induced DWO in CE1 is similar to the Linfa-induced DWO but is 5 m deeper in CE2. A very different feature is found for the anticyclonic eddies, in which the DWO is mostly near zero except during the period when a typhoon passes. The maximum DWO values for ACE1 and ACE2 are −17 m (−23 m) and −20 m (−8 m) during Linfa (Nangka), respectively.
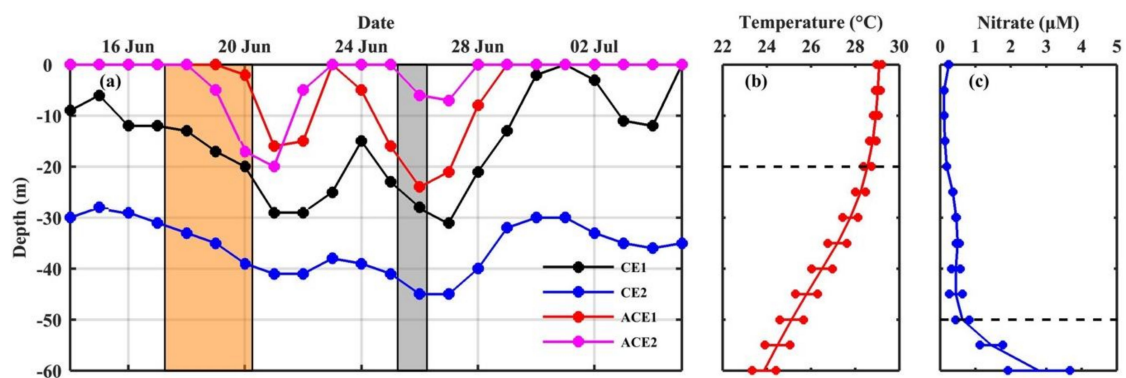

Figure 7. (**a**) Time series of the depth of water origin for CE1 (black), CE2 (blue), ACE1 (red) and ACE2 (magenta). The periods for Linfa and Nangka are indicated by the orange and gray bands, respectively. Climatological profiles for the average and standard deviation of the (**b**) temperature (°C) and (**c**) nitrate concentration (μM) for the regions including all eddies in June. The black dashed lines indicate the mixed layer depth and nutricline.

4. Discussion

　　　Satellite data were used to capture prominent ocean surface responses induced by sequential typhoons in the SCS. Because both typhoons passed over the same region with pre-existing mesoscale eddies, this scenario offers a great opportunity to quantitatively analyze the mechanisms responsible for the typhoon-induced ocean changes and the modulation effect of eddies on those changes. The passage of typhoons drives strong mixing, which simultaneously transports heat downward and nutrients upward [47,48]. In the current study, the typhoons induced a maximum SST cooling equal to 4 °C,

which is slightly weaker than many previous cooling intensities in the same region [3,10,20,34]. For example, Sriver and Huber [49] suggested that the largest typhoon-induced SST depression can reach 8 °C within cyclonic eddies. This disparity is due at least to the weak intensity of both typhoons (neither of them sustained wind speeds larger than 32 m/s), as large changes generally occur in response to typhoons with strong intensities [14]. In addition, both of the cyclonic eddies are characterized by small amplitude and short longevity (Table 1), making them less favorable for driving strong responses when compared with many former studies [13,24]. On the other hand, the impacts of the typhoons on CHL, with a maximum increase equal to 0.2 mg/m^3, are distinct, as depicted by the time series of surface CHL (Figure 5). This is particularly true for the SCS in summer when MLD is shallow [32] and surface water is oligotrophic [33], leading to low chlorophyll [22]. Some studies discovered that typhoon-induced CHL may have increased by a factor of 30 in response to a single typhoon [48], while others revealed that over 50% and 80% of all typhoons in the SCS [16] and Northwest Pacific [28], respectively, cannot even trigger increases in CHL. The selected typhoons in the current study can be considered to be highly representative for conducting investigations on typhoon-induced oceanic responses in the SCS.

Consistent with former studies [17,50,51], large SST and CHL responses are detected to the right of the typhoon tracks (Figure 2). Especially for the SST, typhoon-induced cooling predominantly affects the ocean surface to the right of Linfa and Nangka (Figure 3). Besides the influence of the occurrence of cyclonic eddies on the right of both typhoons (Figure 4), the winds and wind–current resonance on the right side are stronger than those on the left [4]. Huang and Oey [38] used a high-resolution biophysical coupled model and found that submesoscale recirculation cells induce restratification, which decreases turbulence to the right of typhoon tracks. Our results also reveal stronger wind speeds and EPV to the right side of the typhoon tracks to a large extent (Figure 2).

The comparison of the oceanic responses induced by Linfa and Nangka indicates that stronger changes, e.g., SST cooling, are found after the former. This difference is largely attributed to the typhoon features, such as the influence of the wind speed discussed above. The translation speed of Nangka is much higher than that of the majority of typhoons in the SCS [17], resulting in a short forcing time. Thus, the slow wind speed and fast translation speed of Nangka are not favorable for generating large responses [2]. Sun et al. [13] found that a weak typhoon classified as category 1 can still induce evident CHL increases, mainly because a slow translation speed results in a longer forcing time and increased MLD, which consequently contributes to a strong phytoplankton bloom. It is interesting to notice that although these features of Nangka are not favorable for driving oceanic response, prominent changes are also observed for SST (Figure 5), which is highly related with the unique sequential typhoons [35]. Linfa thoroughly mixed the surface ocean structure, and the short period between the two typhoons (Figure 6) does not allow the water to relax back to the initial condition [35]. Furthermore, typhoons can induce prominent surface ocean responses when the ocean is characterized by weak stratification [17]. Thus, another oceanic response would be expected if a sequential typhoon takes place, even if the second event has a weak intensity and fast translation speed (Figures 1 and 5).

The SST cooling and CHL enhancement distributions are not spatially uniform; instead, some locations are associated with large changes (Figure 2). The spatial locations of these large changes are highly coincident with those of cyclonic eddies (Figure 4), indicating that mesoscale eddies can modulate the responses of the ocean to typhoons [52]. Former studies revealed eddy-entrained suspended sediments, phytoplankton and colored dissolved organic matter in the surface ocean, implying that CHL can be largely elevated by typhoons [53]. Phytoplankton blooms then take place 3–4 days after the passage of typhoons associated with the rapid intensification of cyclonic eddies [25]. Zheng et al. [26] found that pre-existing cyclonic eddies in the western North Pacific significantly enhance the SST cooling trend in response to strong typhoons. The presence of warm ocean eddies can effectively block cold, nutrient-rich water from being entrained to the surface [28,54]. In our study, the prominent increases in CHL are highly consistent with pre-existing cyclonic eddies (Figure 2). Additionally, the occurrence of both cyclonic and anticyclonic eddies offers a great opportunity to

evaluate their unique impacts, and clear distinctions are observed among them (Figure 4). Our results indeed indicate that typhoon-induced ocean changes are more prominent in cyclonic eddies than in anticyclonic eddies (Figure 5).

Because mesoscale eddies are ubiquitous in the global ocean [55,56], typhoons can encounter many eddies during their propagations [57]. It is crucially important to understand the ability of mesoscale eddies to regulate ocean responses to typhoons [58]. Pre-existing eddies greatly impact the vertical structure of the water column, and persistent upwelling can be found in cyclonic eddies where the surface water upwells from the subsurface (Figure 7a) [58]. On the other hand, convergence inhibits upwelling within anticyclonic eddies such that subsurface water outcrops to the surface only when a typhoon initiates intensive mixing (Figure 6), while the water column is restratified rapidly after a typhoon (Figure 6b,d). Liu and Tang [59] consistently found that the typhoon-induced CHL increase differs greatly among pre-existing oceanic conditions, with cyclonic and anticyclonic eddies increasing the CHL by approximately 35% and 6%, respectively. Furthermore, the magnitude of SST cooling varies only weakly between the two types of eddies (Figure 5) because typhoon-induced mixing is dominant, while upwelling within cyclonic eddies adds to the typhoon's impact and results in greater cooling at the surface than that within anticyclonic eddies [37].

The intensity of the eddy and the vertical structure of the water column can be influenced by typhoons [60], which in turn modify the subsequent typhoon and its associated ocean responses (Figure 1). Wu and Li [35] investigated sequential typhoons and found that the second typhoon can be weakened by the SST cooling induced by the first typhoon. Indeed, Linfa is intensified to category 4 during its propagation (Figure 1), whereas Nangka is persistently weak throughout its lifespan (Figures 1 and 3c,d). This phenomenon at least occurs because the cooling induced by typhoon Linfa inhibits typhoon Nangka from extracting energy from the ocean surface during its propagation [5]. It is particularly true for regions with pre-existing cyclonic eddies that typhoons intensify the strength of cyclonic eddies after their passage [59,61], leading to stronger upwelling and cooler SST (Figure 5). Besides the impact on the following typhoon, the substantial cooling can even reduce the intensity of the first typhoon as well [5]. In particular, the lingering of Linfa during its early stage can be highly impacted by the cooling induced by itself (Figure 3), which inhibits it from growing into a stronger typhoon (Figure 1).

The delayed CHL responses to the typhoons (Figure 5) indicate that the typhoon-induced nutrient supply is more important than the direct upwelling of subsurface CHL for driving CHL variability [62]. In the current study, the occurrence of a second peak induced by sequential typhoons is determined by the DWO and the nutrient availability at the corresponding depth. However, the second peak presents only if the induced DWO is deeper than that induced by the first typhoon (Figure 7) and there are extra nutrients remaining in the subsurface that are not mixed upward by the first typhoon (Figure 7a,c). Typhoon induced nutrient supply is particularly important to determine the chlorophyll bloom in the SCS as the nutricline is shallow and can be easily mixed up by typhoons [62]. It is important to emphasize that the calculation of DWO based on reanalyzed data is applicable for investigating a typhoon's impact because of the intensive dynamics that take place in a relatively short period [63]. The warming of upwelled water and usage of nutrients for phytoplankton growth can hardly occur during rapid mixing [10]. The proposed method is a valuable approach for quantitatively analyzing the impacts of typhoons on the upper ocean. Although DWO is acquired at the surface (Figure 7), the water does not necessarily need to outcrop at the surface to stimulate phytoplankton responses. For example, some extreme typhoons can induce subsurface CHL blooms even at depths near 100 m, which is greater than the depth of a surface bloom, by transporting nutrients to the euphotic layer [51].

A previous study revealed that oceanic responses, e.g., phytoplankton blooms, induced by Linfa can last for substantially long periods [33]. However, they ignored the occurrence of typhoon Nangka and the impacts of sequential typhoons (Figure 3). In the current study, we evaluate the responses of the ocean to both typhoons and improve our understanding of the corresponding dynamics. The CHL actually returns to its initial condition very rapidly (Figure 5), e.g., 5 days for each bloom, which can

be attributed to regional dynamics and biological processes [59]. In particular, intense radiation warms the ocean within the following three days, and the MLD can be even shallower than that under pre-typhoon conditions (Figure 6). Additionally, restratification at the surface (Figure 5) reduces the nutrient supply and limits phytoplankton growth [16,64], and simultaneous microzooplankton grazing may consume phytoplankton [65], resulting in a rapid decrease in CHL (Figure 4). A comprehensive air–sea interaction model [57] equipped with a biogeochemical cycle can be used in the future to improve our understanding of the regional dynamics and ecological processes [66].

5. Conclusions

Satellite observations clearly reveal the role of eddies in modulating typhoon-induced SST cooling and CHL enhancement in the SCS, while the underlying dynamics are largely dependent of the three-dimensional ocean status. Two sequential typhoons passed over the SCS where four pre-existing eddies occurred; accordingly, this scenario offers an important and unique case study to improve our understanding of typhoon dynamics. Cyclonic eddies can enhance cooling and phytoplankton blooms, while anticyclonic eddies can depress the ocean response. The mechanism of typhoon-induced changes is determined by the relative depths of the MLD, thermocline and nutricline. The DWO is subsequently designed to quantitatively estimate typhoon-induced oceanic responses. The first typhoon can override the impact induced by the second typhoon unless the latter can induce vertical mixing to even greater DWO. The tandem occurrence of typhoons and eddies is greatly important for changing the nutrient supply to the ocean surface and modifying primary production. The proposed method combines satellite observations and reanalysis datasets to offer a comprehensive and quantitative description of typhoon-induced upper ocean responses.

Author Contributions: Visualization, W.J.; conceptualization, C.L., H.L.; investigation, J.H., Q.M., F.L.; data curation, X.C., X.L.; writing—original draft preparation, W.J., Y.W.; writing—review and editing, C.L., Y.W. All authors have read and agreed to the published version of the manuscript.

Conflicts of Interest: The authors declare no conflict of interest.

References

1. Price, J.F. Upper ocean response to a hurricane. *J. Phys. Oceanogr.* **1981**, *11*, 153–175. [CrossRef]
2. Lin, S.; Zhang, W.Z.; Shang, S.P.; Hong, H.S. Ocean response to typhoons in the western North Pacific: Composite results from Argo data. *Deep-Sea Res. Part I* **2017**, *123*, 62–74. [CrossRef]
3. Zhao, H.; Tang, D.; Wang, Y. Comparison of phytoplankton blooms triggered by two typhoons with different intensities and translation speeds in the South China Sea. *Mar. Ecol. Prog. Ser.* **2008**, *365*, 57–65. [CrossRef]
4. Babin, S.M.; Carton, J.A.; Dickey, T.D.; Wiggert, J.D. Satellite evidence of hurricane induced phytoplankton blooms in an oceanic desert. *J. Geophys. Res.* **2004**, *109*, C03043. [CrossRef]
5. Glenn, S.; Miles, T.; Seroka, G.; Xu, Y.; Forney, R.; Yu, F.; Roarty, H.; Schofield, O.; Kohut, J. Stratified coastal ocean interactions with tropical cyclones. *Nat. Commun.* **2016**, *7*, 10887. [CrossRef]
6. Cheung, H.F.; Pan, J.; Gu, Y.; Wang, Z. Remote-sensing observation of ocean responses to Typhoon Lupit in the northwest Pacific. *Int. J. Remote Sens.* **2013**, *34*, 1478–1491. [CrossRef]
7. Emanuel, K.A. Thermodynamic control of hurricane intensity. *Nature* **1999**, *401*, 665–669. [CrossRef]

8. Wang, S.; Li, S.; Hu, J.; Geng, B. Experiments in optimizing simulations of the subsurface chlorophyll maximum in the South China Sea. *J. Mar. Syst.* **2016**, *156*, 1–15. [CrossRef]

9. Wu, R.; Zhang, H.; Chen, D.; Li, C.; Lin, J. Impact of Typhoon Kalmaegi (2014) on the South China Sea: Simulations using a fully coupled atmosphere-ocean-wave model. *Ocean Model* **2018**, *131*, 132–151. [CrossRef]

10. Zhang, H.; Liu, X.; Wu, R.; Liu, F.; Yu, L.; Shang, X.; Qi, Y.; Wang, Y.; Song, X.; Xie, X. Ocean Response to Successive Typhoons Sarika and Haima (2016) Based on Data Acquired via Multiple Satellites and Moored Array. *Remote Sens.* **2019**, *11*, 2360. [CrossRef]

11. Gierach, M.M.; Subrahmanyam, B. Biophysical responses of the upper ocean to major Gulf of Mexico hurricanes in 2005. *J. Geophys. Res. Oceans* **2008**, *113*, C04029. [CrossRef]

12. Price, J.F.; Weller, R.A.; Pinkel, R. Diurnal cycling: Observations and models of the upper ocean response to diurnal heating, cooling, and wind mixing. *J. Geophys. Res.* **1986**, *91*, 8411–8427. [CrossRef]

13. Sun, L.; Yang, Y.; Xian, T.; Lu, Z.; Fu, Y. Strong enhancement of chlorophyll a concentration by a weak typhoon. *Mar. Ecol. Prog. Ser.* **2010**, *404*, 39–50. [CrossRef]

14. Zhao, H.; Pan, J.; Han, G.; Devlin, A.T.; Zhang, S.; Hou, Y. Effect of a fast-moving tropical storm Washi on phytoplankton in the northwestern South China Sea. *J. Geophys. Res. Oceans* **2017**, *122*, 3404–3416. [CrossRef]

15. Mei, W.; Lien, C.C.; Lin, I.I.; Xie, S.P. Tropical cyclone-induced ocean response: A comparative study of the South China Sea and Tropical Northwest Pacific. *J. Clim.* **2015**, *28*, 5952–5968. [CrossRef]

16. Pan, G.; Chai, F.; Tang, D.; Wang, D. Marine phytoplankton biomass responses to typhoon events in the South China Sea based on physical-biogeochemical model. *Ecol. Modell.* **2017**, *356*, 38–47. [CrossRef]

17. Zhang, H.; Wu, R.; Chen, D.; Liu, X.; He, H.; Tang, Y.; Ke, D.; Shen, Z.; Li, J.; Xie, J.; et al. Net modulation of upper ocean thermal structure by Typhoon Kalmaegi (2014). *J. Geophys. Res. Oceans* **2018**, *123*, 7154–7171. [CrossRef]

18. Han, G.; Ma, Z.; Chen, N. Hurricane Igor impacts on the stratification and phytoplankton bloom over the Grand Banks. *J. Mar. Syst.* **2012**, *100*, 19–25. [CrossRef]

19. Tang, S.; Dong, Q.; Liu, F. Climate-driven chlorophyll-a concentration interannual variability in the South China Sea. *Theor. Appl. Climatol.* **2011**, *103*, 229–237. [CrossRef]

20. Zhang, W.Z.; Wang, H.; Chai, F.; Qiu, G. Physical drivers of chlorophyll variability in the open South China Sea. *J. Geophys. Res. Oceans* **2016**, *121*, 7123–7140. [CrossRef]

21. Geider, R.J.; MacIntyre, H.L.; Kana, T. A dynamic regulatory model of phytoplanktonic acclimation to light, nutrients, and temperature. *Limnol. Oceanogr.* **1998**, *43*, 679–694. [CrossRef]

22. Yu, Y.; Xing, X.; Liu, H.; Yuan, Y.; Wang, Y.; Chai, F. The variability of chlorophyll-a and its relationship with dynamic factors in the basin of the South China Sea. *J. Mar. Syst.* **2019**, *200*, 103230. [CrossRef]

23. Pan, J.; Sun, Y. Estimate of Ocean Mixed Layer Deepening after a Typhoon Passage over the South China Sea by Using Satellite Data. *J. Phys. Oceanogr.* **2013**, *43*, 498–506. [CrossRef]

24. Chelton, D.B.; Schlax, M.G.; Samelson, R.M. Global observations of nonlinear mesoscale eddies. *Prog. Oceanogr.* **2011**, *91*, 167–216. [CrossRef]

25. Walker, N.D.; Leben, R.R.; Balasubramanian, S. Hurricane-forced upwelling and chlorophyll a enhancement within cold-core cyclones in the Gulf of Mexico. *Geophys. Res. Lett.* **2005**, *32*, 109–127. [CrossRef]

26. Zheng, Z.-W.; Ho, C.-R.; Zheng, Q.; Lo, Y.-T.; Kuo, N.-J.; Gopalakrishnan, G. Effects of preexisting cyclonic eddies on upper ocean responses to Category 5 typhoons in the western North Pacific. *J. Geophys. Res.* **2010**, *115*, C09013. [CrossRef]

27. Shi, W.; Wang, M. Satellite observations of asymmetrical physical and biological responses to Hurricane Earl. *Geophys. Res. Lett.* **2011**, *38*, 2–6. [CrossRef]

28. Lin, I.I. Typhoon-induced phytoplankton blooms and primary productivity increase in the western North Pacific subtropical ocean. *J. Geophys. Res.* **2012**, *117*, C03039. [CrossRef]

29. Lu, Z.; Gan, J.; Dai, M.; Zhao, X.; Hui, C.R. Nutrient transport and dynamics in the South China Sea: A modeling study. *Prog. Oceanogr.* **2020**, *183*, 102308. [CrossRef]

30. Wang, G.; Su, J.; Ding, Y.; Chen, D. Tropical cyclone genesis over the south China sea. *J. Mar. Syst.* **2007**, *68*, 318–326. [CrossRef]

31. Wang, Y.; Yu, Y.; Zhang, Y.; Chai, F. Distribution and variability of sea surface temperature fronts in the South China Sea. *Estuar. Coast. Shelf Sci.* **2020**, *240*, 106793. [CrossRef]

32. Hu, J.; Kawamura, H.; Hong, H.; Qi, Y. A Review on the Currents in the South China Sea: Seasonal Circulation, South China Sea Warm Current and Kuroshio Intrusion. *J. Oceanogr.* **2000**, *56*, 607–624. [CrossRef]

33. Xiu, P.; Chai, F.; Shi, L.; Xue, H.; Chao, Y. A census of eddy activities in the South China Sea during 1993–2007. *J. Geophys. Res.* **2010**, *115*, C03012. [CrossRef]

34. Sun, L.; Li, Y.X.; Yang, Y.J.; Wu, Q.; Chen, X.T.; Li, Q.Y.; Li, Y.-B.; Xian, T. Effects of super typhoons on cyclonic ocean eddies in the western North Pacific: A satellite data-based evaluation between 2000 and 2008. *J. Geophys. Res. Oceans* **2014**, *119*, 5585–5598. [CrossRef]

35. Wu, R.; Li, C. Upper ocean response to the passage of two sequential typhoons. *Deep Sea Res. Part I* **2018**, *132*, 68–79. [CrossRef]

36. Chen, Y.Q.; Tang, D.L. Eddy-feature phytoplankton bloom induced by a tropical cyclone in the South China Sea. *Int. J. Remote Sens.* **2012**, *33*, 7444–7457. [CrossRef]

37. Liu, F.; Tang, S. Influence of the interaction between typhoons and oceanic mesoscale eddies on phytoplankton blooms. *J. Geophys. Res. Oceans* **2018**, *123*, 2785–2794. [CrossRef]

38. Huang, S.M.; Oey, L.Y. Right-side cooling and phytoplankton bloom in the wake of a tropical cyclone. *J. Geophys. Res. Oceans* **2015**, *120*, 5735–5748. [CrossRef]

39. Jyothi, L.; Joseph, S. Surface and sub-surface ocean response to Tropical Cyclone Phailin: Role of pre-existing oceanic features. *J. Geophys. Res. Oceans* **2019**, *124*, 6515–6530. [CrossRef]

40. Vidya, P.J.; Santosh, D.; Mani Murali, R. Contrasting Chl-a responses to the tropical cyclones Thane and Phailin in the Bay of Bengal. *J. Mar. Syst.* **2017**, 103–114. [CrossRef]

41. Chassignet, E.P.; Hurlburt, H.E.; Smedstad, O.M.; Halliwell, G.R.; Hogan, P.J.; Wallcraft, A.J.; Baraille, R.; Bleck, R. The HYCOM (Hybrid Coordinate Ocean Model) data assimilative system. *J. Mar. Syst.* **2007**, *65*, 60–83. [CrossRef]

42. Cummings, J.A.; Smedstad, O.M. *Variational Data Assimilation for the Global Ocean. Data Assimilation for Atmospheric, Oceanic and Hydrologic Applications*; Springer: Berlin/Heidelberg, Germany, 2013; Volume II, pp. 303–343. [CrossRef]

43. Zhang, W.Z.; Hong, H.S.; Yan, X.H. Typhoons enhancing northward transport through the Taiwan Strait. *Cont. Shelf Res.* **2013**, *56*, 13–25. [CrossRef]

44. Sanford, T.B.; Price, J.F.; Girton, J.B. Upper ocean response to Hurricane Frances (2004) observed by profiling EM-APEX floats. *J. Phys. Oceanogr.* **2011**, *41*, 1041–1056. [CrossRef]

45. Obata, A.; Ishizaka, J.; Endoh, M. Global verification of critical depth theory for phytoplankton bloom with climatological in situ temperature and satellite ocean color data. *J. Geophys. Res.* **1996**, *101*, 20657–20667. [CrossRef]

46. Van Wambeke, F.; Ghiglione, J.; Nedoma, J.; Mevel, G.; Raimbault, P. Short scale variations in nutrients, ectoenzymatic activities and bottom-up effects on bacterial production and community structure during late summer-autumn transition in the open NW Mediterranean Sea. *Biogeosci. Discuss.* **2009**, *6*, 687–727. [CrossRef]

47. Emanuel, K.A. Contribution of tropical cyclones to meridional heat transport by the oceans. *J. Geophys. Res.* **2001**, *106*, 14771–14782. [CrossRef]

48. Lin, I.; Liu, W.T.; Wu, C.C.; Wong, G.T.F.; Hu, C.; Chen, Z.; Liang, W.D.; Yang, Y.; Liu, K.K. New evidence for enhanced ocean primary production triggered by tropical cyclone. *Geophys. Res. Lett.* **2003**, *30*, 1718. [CrossRef]

49. Sriver, R.L.; Huber, M. Observational evidence for an ocean heat pump induced by tropical cyclones. *Nature* **2007**, *447*, 577–580. [CrossRef]

50. Shibano, R.S.; Yamanaka, Y.; Okada, N.; Chuda, T.; Suzuki, S.; Niino, H. Responses of marine ecosystem to typhoon passages in the western subtropical North Pacific. *Geophys. Res. Lett.* **2011**, *38*, L18608. [CrossRef]

51. Ye, H.J.; Sui, Y.; Tang, D.L.; Afanasyev, Y.D. A Subsurface Chlorophyll a Bloom Induced by Typhoon in the South China Sea. *J. Mar. Syst.* **2013**, *128*, 138–145. [CrossRef]

52. Xu, F.; Yao, Y.; Oey, L.; Lin, Y. Impacts of pre-existing ocean cyclonic circulation on sea surface chlorophyll-a concentrations off northeastern Taiwan following episodic typhoon passages. *J. Geophys. Res. Oceans* **2017**, *122*, 6482–6497. [CrossRef]

53. Zheng, G.M.; Tang, D.L. Offshore and nearshore chlorophyll increases induced by typhoon winds and subsequent terrestrial rainwater runoff. *Mar. Ecol. Prog. Ser.* **2007**, *333*, 61–74. [CrossRef]

54. Lin, I.I.; Chun-Chieh, W.U.; Emanuel, K.A.; Lee, I.H.; Wu, C.R.; Pun, I.F. The interaction of super typhoon Maemi (2003) with a warm ocean eddy. *Mon. Weather Rev.* **2005**, *133*, 2635–2649. [CrossRef]

55. Gaube, P.; Chelton, D.B.; Samelson, R.M.; Schlax, M.G.; Oneill, L.W. Satellite Observations of Mesoscale Eddy-Induced Ekman Pumping. *J. Phys. Oceanogr.* **2015**, *45*, 104–132. [CrossRef]

56. Sun, W.; Dong, C.; Tan, W.; Liu, Y.; He, Y.; Wang, J. Vertical Structure Anomalies of Oceanic Eddies and Eddy-Induced Transports in the South China Sea. *Remote Sens.* **2018**, *10*, 795. [CrossRef]

57. Yue, X.; Zhang, B.; Liu, G.; Li, X.; Zhang, H.; He, Y. Upper Ocean Response to Typhoon Kalmaegi and Sarika in the South China Sea from Multiple-Satellite Observations and Numerical Simulations. *Remote Sens.* **2018**, *10*, 348. [CrossRef]

58. Ning, J.; Xu, Q.; Zhang, H.; Wang, T.; Fan, K. Impact of Cyclonic Ocean Eddies on Upper Ocean Thermodynamic Response to Typhoon Soudelor. *Remote Sens.* **2019**, *11*, 938. [CrossRef]

59. Liu, Y.; Tang, D.; Evgeny, M. Chlorophyll Concentration Response to the Typhoon Wind-Pump Induced Upper Ocean Processes Considering Air-Sea Heat Exchange. *Remote Sens.* **2019**, *11*, 1825. [CrossRef]

60. Lu, Z.; Wang, G.; Shang, X. Response of a preexisting cyclonic ocean eddy to a typhoon. *J. Phys. Oceanogr.* **2016**, *46*, 2403–2410. [CrossRef]

61. Yang, Y.J.; Sun, L.; Liu, Q.; Xian, T.; Fu, Y. The biophysical responses of the upper ocean to the typhoons Namtheun and Malou in 2004. *Int. J. Remote Sens.* **2010**, *31*, 4559–4568. [CrossRef]

62. Pan, J.Y.; Huang, L.; Devlin, A.T.; Lin, H. Quantification of Typhoon-Induced Phytoplankton Blooms Using Satellite Multi-Sensor Data. *Remote Sens.* **2018**, *10*, 318. [CrossRef]

63. Zhang, S.; Xie, L.; Hou, Y.; Zhao, H.; Qi, Y.; Yi, X. Tropical storm-induced turbulent mixing and chlorophyll-a enhancement in the continental shelf southeast of Hainan Island. *J. Mar. Syst.* **2014**, *129*, 405–414. [CrossRef]

64. Baranowski, D.B.; Flatau, P.J.; Chen, S.; Black, P.G. Upper ocean response to the passage of two sequential typhoons. *Ocean Sci.* **2014**, *10*, 559–570. [CrossRef]

65. Zhou, L.; Tan, Y.; Huang, L.; Huang, J.; Liu, H.; Lian, X. Phytoplankton growth and microzooplankton grazing in the continental shelf area of northeastern South China Sea after Typhoon Fengshen. *Cont. Shelf Res.* **2011**, *31*, 1663–1671. [CrossRef]

66. Chai, F.; Johnson, K.S.; Claustre, H.; Xing, X.; Wang, Y.; Boss, E.; Riser, S.; Fennel, K.; Schofield, O.; Sutton, A. Monitoring ocean biogeochemistry with autonomous platforms. *Nat. Rev. Earth Environ.* **2020**, 315–326. [CrossRef]